PHYSICAL REVIEW E VOLUME 51, NUMBER 1 JANUARY 1995

Effective bandwidth and the Kompfner dip for cyclotron autoresonance maser amplifiers

C. S. Kou and K. R. Chu
Department of Physics, National Tsing Hua University, Hsinchu, Taiwan, Republic of China

D. B. McDermott and N. C. Luhmann, Jr.
Department of Applied Science, University of California, Davis, California 95616
(Received 6 June 1994; revised manuscript received 16 September 1994)

This paper investigates the inadequacy of using the growth rate from the dispersion relation to represent the bandwidth of a cyclotron autoresonance maser (CARM) amplifier. It is shown that the dispersion relation can accurately predict the amplifier's bandwidth, but at least three waves that the electron beam couples to must be retained in the calculation. Interference between these waves must be included. The bandwidth of the coupling coefficient for the forward growing wave can be much narrower than the bandwidth of this wave's growth rate. In addition, the input signal has been observed to be almost totally absorbed by the electron beam at a specific frequency which is a function of the operating conditions. This phenomenon is caused by the beating between the forward constant amplitude wave and the forward growing wave. It is analogous to the Kompfner dip in a conventional linear beam traveling wave tube and can, therefore, become a useful diagnostic for determining the experimental parameters of a CARM amplifier.

PACS number(s): 41.75.−i, 42.52.+x

I. INTRODUCTION

Considerable interest has arisen in developing high power sources of radiation in millimeter and submillimeter regime. One of the promising candidates is the electron cyclotron autoresonance maser (CARM) [1–7]. In this device, a relativistic electron beam interacts with a right circularly polarized electromagnetic wave, gyrating along a magnetic field. Resonance between the electrons and the wave takes place when $\omega = k_z v_z + \Omega_c$, where ω is the angular frequency of the wave, $\Omega_c = eB/\gamma m_0 c$ is the relativistic electron cyclotron frequency, γ is the electron Lorentz factor, k_z and v_z are the propagation constant of the wave and the drift velocity of the electrons along the magnetic field. The variation of the Doppler shift and the relativistic cyclotron frequency in the above resonance condition results in axial bunching and azimuthal bunching processes, respectively. These two bunching processes cancel and compete with each other [8].

The Doppler shift term $k_z v_z$ becomes significant for the CARM interaction. If the wave phase velocity is equal to the speed of light, it has been shown [2] that when electrons lose their energy to the wave, the increase in Ω_c will be exactly compensated by a decrease in $k_z v_z$. The electrons will then maintain their resonance with the wave over a long interaction time. However, this autoresonance condition nevertheless results in a low growth rate due to the exact cancellation between the axial and azimuthal bunching. Consequently, the CARM is usually operated with the wave phase velocity slightly larger than the speed of light to avoid this exact compensation between the two bunching mechanisms [2,8].

One important physical issue addressed in Ref. [9] is concerned with the effective bandwidth of the CARM. It has been found that the bandwidth of a CARM amplifier, predicted by the dispersion relation, can exceed one octave, whereas, the particle simulation shows that the bandwidth is substantially less. Good agreement exists only near the frequency at which the electron beam is well synchronized with the waveguide mode. Therefore, the discrepancy between linear theory and particle simulation has been attributed to the invalidity of the linear theory at frequencies outside the close resonance region [8]. This issue is re-addressed and examined in this study. A different conclusion is obtained. The growth rate solved by the dispersion relation is verified to remain valid even when electrons are not closely synchronous with the wave. The discrepancy between linear theory and particle simulation is demonstrated to be caused by launching loss effects, which can become extremely large and severely deteriorates the bandwidth of a CARM amplifier. It is well known that the launching loss can significantly reduce the gain of traveling wave devices [10,11]. However, such drastically detrimental effects on the bandwidth of a CARM had not heretofore been explored.

The launching loss is due to the fact that four possible solutions are available for the wave number at any real frequency when solving the dispersion relation for a CARM [9,12–14]. These solutions correspond to four waves excited by the interaction between the wave and electrons and only one of these four waves can spatially grow along the tube. Furthermore, they must all be present to satisfy the initial boundary conditions in a finite or semifinite system. In other words, the input rf signal actually couples into four waves in the beginning of the interaction. The dispersion relation can only be used for predicting the growth rates and propagation constants of these four waves. However, it cannot provide information regarding the coupling of the input

power to each of the four waves.

Meanwhile, the input signal has been observed to be almost totally absorbed by the electron beam at a specific frequency for each operating condition. This phenomenon is well known in conventional linear beam traveling-wave-tube (TWT) amplifiers as the Kompfner dip [15,16]. The Kompfner dip has become a useful technique in determining the characteristics of a TWT. This dip is analogously capable of becoming an experimental technique to characterize a CARM amplifier. The importance of this study is to provide not only the physical insight into the effective bandwidth of a CARM but also a potential experimental method to determine the operating conditions of a CARM.

In this paper, the linear theory developed in Refs. [17–19] is employed, where the Laplace transformation is used for solving the Maxwell-Vlasov integro-differential equation. Hence, this theory includes the launching loss in the analysis. The same technique has also been used for analyzing multimode interactions in CARM amplifiers in Refs. [20] and [21]. In addition, a fast-time-scale nonlinear theory, which does not assume that $\omega-k_z v_z-s\Omega_e/\gamma\simeq 0$, is developed to verify the accuracy of the slow-time-scale linear theory. It is found that the slow-time-scale theory is valid even for interactions quite far from resonance.

II. LINEAR THEORY

The linear theory is briefly described in the following. We consider either an annular or an axis-encircling electron beam traveling along a cylindrical waveguide, guided by an external magnetic field. A circularly polarized TE_{mn} waveguide mode is injected into the waveguide to interact with the electron beam. The spatial evolution of the wave along the waveguide can be determined as follows [18,19]:

$$F(z)=\sum_i \left[\frac{F(0)N(k_{zi})+F'(0)}{jD'(k_{zi})}\right]\exp(-jk_{zi}z)\ , \tag{1}$$

where k_{zi} is the ith root of the following equation:

$$D(\omega,k_z)=\frac{\omega^2}{c^2}-k_z^2-k_{mn}^2-\frac{16\pi^3e^2C_{mn}^2}{m_0c^2}\sum_s^{\infty}\int_0^{r_c^{\max}} r_c dr_c \int_0^{\infty} p_\perp dp_\perp \int_{-\infty}^{+\infty} dp_z \frac{f_0}{\gamma}$$
$$\times\left[\frac{-\beta_\perp^2(\omega^2-k_z^2c^2)H_{sm}(k_{mn}r_c k_{mn}r_L)}{(\omega-k_2v_2-s\Omega_{c0}/\gamma)^2}+\frac{(\omega-k_zv_z)T_{sm}(k_{mn}r_c k_{mn}r_L)}{(\omega-k_zv_z-s\Omega_{c0}/\gamma)}-\frac{k_{mn}v_\perp U_{sm}(k_{mn}r_c k_{mn}r_L)}{(\omega-k_zv_z-s\Omega_{c0}/\gamma)}\right]=0\ , \tag{2}$$

$D'(k_z)=dD(k_z)/dk_z$, and

$$N(k_z)=-jk_z+j\frac{16\pi^3e^2C_{mn}^2}{m_0c}\sum_s^{\infty}\int_0^{r_c^{\max}} r_c dr_c \int_0^{\infty} p_\perp dp_\perp \int_{-\infty}^{\infty} dp_z \frac{f_0}{\gamma}\left[\frac{-v_\perp^2k_z\omega H_{sm}(k_{mn}r_c k_{mn}r_L)}{(\omega-k_zv_z-s\Omega_{c0}/\gamma)^2}+\frac{v_zT_{sm}(k_{mn}r_c k_{mn}r_L)}{(\omega-k_zv_z-s\Omega_{c0}/\gamma)}\right]\ . \tag{3}$$

The definitions of $H_{sm}(x,y)$, $T_{sm}(x,y)$, and $U_{sm}(x,y)$ are given as follows:

$$H_{sm}(x,y)=J_{s-m}^2(x)J_s'^2(y)\ ,$$

$$T_{sm}(x,y)=2H_{sm}(x,y)+yJ_s'(y)\left\{2J_s'(y)-J_s(y)\left[\frac{1}{x}J_{s-m}(x)J_{s-m}'(x)+J_{s-m}'^2(x)+J_{s-m}(x)J_{s-m}''(x)\right]\right\}\ ,$$

and

$$U_{sm}(x,y)=-\tfrac{1}{2}yJ_s'(y)\{J_{s-1}(y)[J_{s-m-1}^2(x)-J_{s-m}^2(x)]+J_{s+1}(y)[J_{s-m+1}^2(x)-J_{s-m}^2(x)]\}\ . \tag{4}$$

In the above, f_0 is the equilibrium distribution function of an electron beam, k_z is the complex axial wave number, $k=\omega/c$. $C_{mn}^2=[J_m^2(x_{mn})(1-m^2/x_{mn}^2)]^{-1}$, x_{mn} is the nth root of the Bessel function $J_m'(x)$, r_ω is the waveguide radius, $k_{mn}=x_{mn}/r_\omega$, r_L is the electron Larmor radius, r_c is the guiding center radius, $\Omega_{c0}=eB_0/mc$ is the electron cyclotron frequency and s is the cyclotron harmonic number. $F(0)$ and $F'(0)$ are the amplitudes of

the wave and its first derivative at $z=0$.

The power flow in the waveguide can be calculated by integrating the Ponyting vector over the waveguide cross section, which yields

$$P_w=\mathrm{Re}\left\{\int dA\frac{c}{8\pi}(EB^*)\right\}=\frac{c^2}{8\pi}\frac{1}{\omega k_{mn}^2}\mathrm{Re}\{F(z)jF'(z)^*\}\ . \tag{5}$$

The linear gain is then given by

$$G(z)=\frac{P_w(z)}{P_w(0)}=\frac{\mathrm{Im}\{F(z)F'(z)^*\}}{\mathrm{Im}\{F(0)F'(0)^*\}}\ . \tag{6}$$

In deriving Eq. (1), small signal assumptions have been made so that the first-order perturbations of all quantities are smaller than the zero-order quantities and the contributions from the higher-order terms are negligible in the analysis. In addition, the operating conditions are assumed to be $\omega-k_z v_z-s\Omega/\gamma\approx 0$ so that the contributions from other cyclotron harmonics can be neglected except for the sth harmonic. Equation (1) results from applying the Laplace transformation to the linearized Maxwell-Vlasov equation. The initial boundary condition can subsequently be taken into account. Equation (2) is notably the well-known dispersion relation [9] for the cyclotron maser instability that originates from the coupling between the waveguide mode ($\omega^2/c^2-k_z^2-k_{mn}^2=0$) and the beam mode ($\omega-k_z v_z-s\Omega_{c0}/\gamma=0$). It can, therefore, determine the waves to be excited and also their growth rates. Equation (2) further indicates that four roots can be obtained by solving the dispersion relation, corresponding to four different waves. They are a backward constant amplitude wave, a forward constant amplitude wave, a forward growing wave and a forward decaying wave. The last two waves correspond to a pair of complex conjugate solutions to the dispersion relation. On the other hand, the terms inside the square brackets in Eq. (1) represent the coupling of the waves by the input signal.

III. NONLINEAR THEORY

A self-consistent nonlinear simulation model is used to verify the validity of the linear theory described above. We consider a relativistic electron beam traveling through a waveguide, guided by an external dc magnetic field applied along the z axis. The B_z component of the circularly polarized TE_{mn} waveguide mode is given by

$$B_z=B_0(z)J_m(k_{mn}r)\cos(\omega t-m\theta-\beta z+\Phi(z))\ , \tag{7}$$

where $\Phi(z)$ is the wave phase. With a source current $\tilde{J}$, Maxwell's equations become

$$\nabla^2 B-\frac{1}{c^2}\frac{\partial^2}{\partial t^2}B=-\frac{4\pi}{c}\nabla\tilde{J}\ , \tag{8}$$

where B is the wave magnetic field. Taking the z component of Eq. (8) and substituting Eq. (7) for B_z, the circuit equations that govern the spatial rate of change of the wave amplitude and phase can be determined by straightforward algebra and are given by

$$\{B_0''(z)+B_0(z)[2\Phi'(z)\beta-\Phi'(z)^2]\}=\frac{2}{cS_{mn}}\oint ds\,\langle \tilde{J}_\theta k_{mn}J_m'(k_{mn}r)\cos(\omega t-\beta z-m\theta+\Phi(z))$$
$$-\frac{m}{r}\tilde{J}_r J_m(k_{mn}r)\sin(\omega t-\beta z-m\theta+\Phi(z))\rangle_t \tag{9}$$

$$\{2B_0'(z)[\beta-\Phi'(z)]-B_0(z)\Phi''(z)\}=\frac{2}{cS_{mn}}\oint_s ds\,\langle \tilde{J}_\theta k_{mn}J_m'(k_{mn}r)\sin(\omega t-\beta z-m\theta+\Phi(z))$$
$$+\frac{m}{r}\tilde{J}_r J_m(k_{mn}r)\cos(\omega t-\beta z-m\theta+\Phi(z))\rangle_t\ , \tag{10}$$

where $S_{mn}=r_\omega^2 J_m^2(x_{mn})(1-m^2/x_{mn}^2)$, and $\tilde{J}_r$ and $\tilde{J}_\theta$ are the radial and azimuthal components of the current and $\langle f\rangle_t$ is defined as

$$\langle f\rangle_t=\frac{\omega}{2\pi}\int_0^{2\pi/\omega} f\,dt\ .$$

The electron dynamics are required for evaluating the current source terms on the right-hand sides of Eq. (9) and (10). They are governed by the Lorentz force and are given by

$$\frac{dp}{dt}=-eE-ev\times B\ . \tag{11}$$

The electrons are subject to the forces imposed by the wave and external dc magnetic field. It is worth noting that the exact field components will be used in evaluating Eq. (9) without any simplification based on the resonance condition. Consequently, the equations are valid for any synchronism situation between the wave and electron beam.

The two-wave equations coupled with the equations of motion for each test electron consist of a self-consistent simulation model. They comprise a system of $7N_p+4$ simultaneous ordinary differential equations (N_p is the number of test electrons) and are solved by the Runge-Kutta method. The precision of the simulation is monitored by the energy conservation law and the redundant equation of motion.

IV. RESULTS AND DISCUSSION

Throughout this section, we will consider an electron beam interacting with a TE_{01} waveguide mode at the first

cyclotron harmonic. The system parameters are: beam voltage $V_b=700$ kV, beam current $I_b=7$ A, $\alpha(v_\perp/v_z)=0.525$, $r_c/r_\omega=0.48$, and $B_0=1.24875B_g$, where the grazing magnetic field B_g is the value at which the cyclotron beam mode $(\omega-kv_z-s\Omega_{c0}/\gamma=0)$ is tangent to the waveguide mode $(\omega^2/c^2-k_z^2-k_{mn}^2=0)$.

The solutions of the dispersion relation [Eq. (2)] are depicted in Fig. 1. The real parts (k_{zr}) and imaginary parts (k_{zi}) of the solved complex wave numbers are displayed in Fig. 1(a) and Fig. 1(b), respectively. They represent the propagation constant and the growth or decay rate of the corresponding wave. With $B_0=1.248\,75B_g$, the beam mode intersects with the waveguide mode at two frequencies which are 190.26 GHz and 542.62 GHz. Figure 1(b) illustrates that an extremely broad unstable bandwidth expands over the two intersection points. This study will focus on the bandwidth around the upper intersection point where CARM interactions can occur.

Figure 2 illustrates the total gain versus frequency of this amplifier with a 17.5-cm interaction length. In this figure, the solid line is the gain predicted by our linear theory, where all four waves are taken into account. The dashed line also representing the total gain is based on the assumption that the input signal totally couples to the forward growing wave. The results demonstrate a large discrepancy between these two predictions. To verify the results calculated by our linear theory, the self-consistent model described in Sec. III has been used to simulate the amplification of the wave. The calculated results have also been plotted in Fig. 2, showing perfect agreement with the linear theory. Further confirmation is provided in Fig. 3, where the evolution of a 400 GHz wave along the waveguide is plotted as calculated by the linear theory and the self-consistent simulation. To fully illustrate the growth of the wave, the interaction length has been extended to 60 cm. After an initial region of periodic variation, the wave is eventually observed to grow exponentially at a rate exactly the value predicted by the

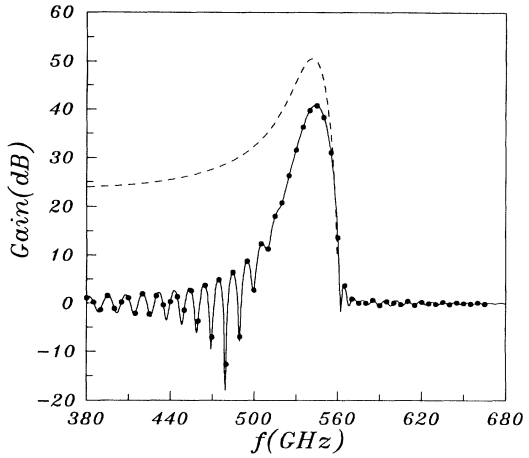

FIG. 2. The gain versus frequency for a TE_{01} mode CARM amplifier, predicted by the four-wave model (solid curve), the nonlinear simulation (dots) and the growth rate of the forward growing wave from the dispersion relation (dashed curve). The interaction length is 17.5 cm and other parameters are the same as in Fig. 1.

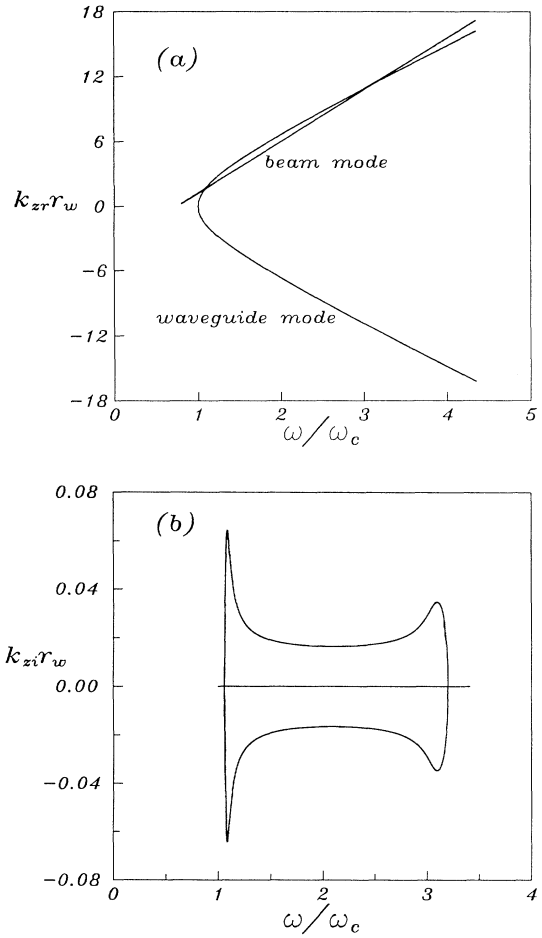

FIG. 1. The (a) real part and (b) imaginary part of the wave number versus frequency for a TE_{01} mode CARM amplifier: $V_b=700$ kV, $I_b=7$ A, $\alpha=0.525$, $B=1.20875B_g$, $r_\omega=0.10448$ cm, $s=1$.

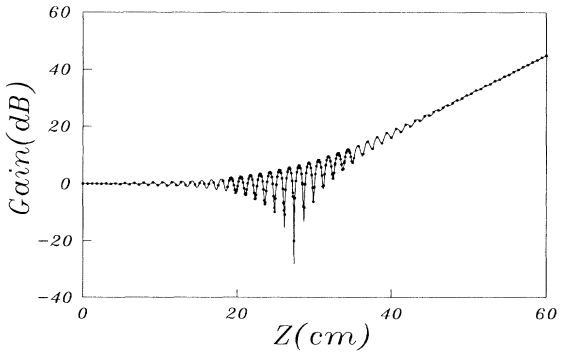

FIG. 3. The spatial power growth of a 400 GHz wave in a CARM amplifier from the nonlinear simulation (solid curve) and the linear theory (dots). The system parameters are the same as in Fig. 1.

dispersion relation. Note that the wave frequency of 400 GHz is 150 GHz from the upper intersection point between the beam mode and the waveguide mode and is located in a region where the wave and electron are not well synchronized. The agreement demonstrated above has strongly confirmed the validity of the four-wave model and also the adequacy of the dispersion relation.

The discrepancy shown in Fig. 2 can be explained by considering the coupling of the four waves at the initial position of the interaction which are the absolute amplitudes of the square brackets in Eq. (1). The relative coupling coefficients for each wave for the operating parameters corresponding to Fig. 2 are plotted in Fig. 4. The coupling to the backward wave is too weak to be shown and has not been included. In addition, the coupling to the forward growing and forward decaying waves are equal. Therefore, only two curves are shown. From this figure, the coupling to the unstable wave only becomes effective around the intersection point (549.62 GHz) and the constant amplitude forward wave is dominant at a frequency relatively far from the intersection point. In other words, the effective bandwidth only exists around the intersection point while the unstable waves outside this region cannot grow to a significant amplitude in a reasonable interaction length because their initial amplitudes are too small. The periodic variation in Fig. 3, which occurs for frequencies below the effective bandwidth, is due to the beating between the forward constant amplitude wave and the forward growing wave. This issue is further discussed in the following paragraphs.

The physical reason for the weak coupling of the unstable wave can be understood by inspecting the complex wave numbers obtained from the dispersion relation. Complex conjugate pairs with strong coupling between the wave and electron beam only occur near the intersection point. The complex conjugate solutions found in other regions belong to the beam modes which travel much faster than the "cold" circuit wave (i.e., the TE_{01} waveguide mode in the absence of an electron beam). On the other hand, the forward constant amplitude wave propagates rather close to the cold circuit wave in these regions. From a physical point of view, the wave with a propagation constant closest to that of the cold waveguide mode (which is injected into the interaction region at $z=0$), is most easily excited among those four waves since it has the same wave impedance of the input signal. Thus, the forward constant amplitude wave becomes dominant over the forward growing wave at frequencies relatively far from the intersection point.

Compared with linear beam traveling wave tubes (TWT) or gyrotron traveling-wave tubes (gyro-TWT), the launching losses of a CARM amplifier are apparently much more drastic. In a TWT or gyro-TWT, the unstable wave is always the major component of the four-wave mixture. Reductions of the interaction gain certainly occur, but severe curtailment of the bandwidth has not been observed. Furthermore, the launching loss actually falls off on both edges of the unstable bandwidth in those two devices and tends to preserve the bandwidth. The reason for the different behavior of the launching loss is due to the way that the beam mode contacts the waveguide mode. In a TWT or gyro-TWT, the beam mode is usually set to be almost tangential to the waveguide mode such that electrons can maintain close resonance with the wave over a wide frequency range. However, the beam mode in a CARM amplifier intersects with the waveguide mode as shown in Fig. 1. Resonance is weak away from the intersection.

It is worth noting that a sharp negative gain dip appears on the left side of the effective bandwidth in Fig. 2. This dip simply indicates that the input power at this frequency is almost totally absorbed by the electron beam at $z=17.5$ cm. Figure 5 shows the evolution of the four waves along the waveguide at 479.57 GHz where the dip takes place. Since the wavelength is only 0.067 cm, each

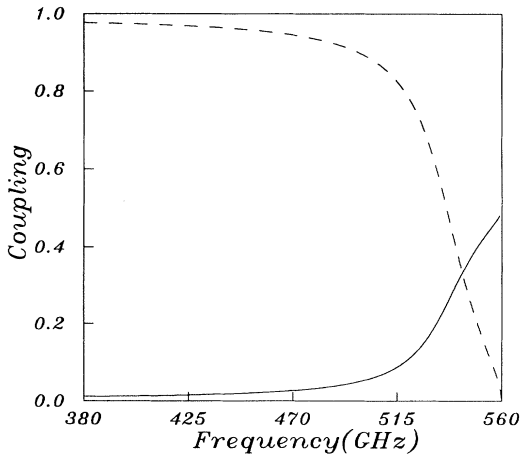

FIG. 4. The relative coupling coefficients of the forward constant amplitude wave (dashed curve) and the forward growing wave (solid curve). The system parameters are the same as in Fig. 1.

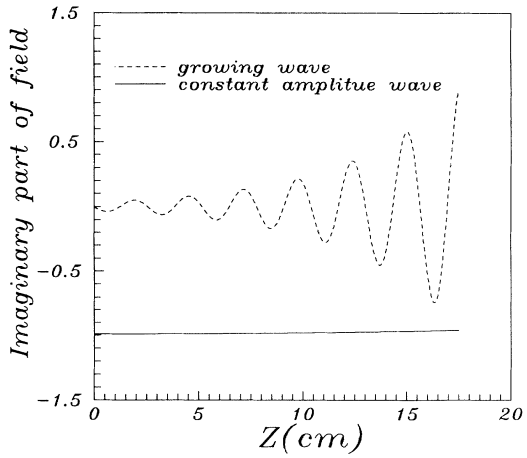

FIG. 5. The spatial evolution of the imaginary part of the amplitude for the forward constant amplitude wave (solid line) and the forward growing wave (dashed line) for a 479.57 GHz wave in a CARM amplifier. Each wave has been divided by $\exp(-jk_0z)$.

wave has been divided by $\exp(-jk_{z0}z)$ to eliminate the fast varying term, where k_{z0} is the wave number of the cold waveguide. Consequently, the forward constant amplitude wave does not display a periodic motion since its propagation constant is almost equal to that of the cold waveguide mode. This plot again indicates that the absorption dip is simply due to the beatings between the forward constant amplitude wave and the forward growing wave.

This total absorption of the input signal has been observed to occur only at a specific frequency for each operating condition. Figure 6 shows that total absorption would occur at a higher frequency for a shorter interaction length. Since the coupling of the forward growing wave increases with the frequency as indicated in Fig. 4, the length for it to catch up to the forward constant amplitude wave becomes shorter.

This phenomenon of total absorption is analogous to the Kompfner dip which occurs in conventional linear beam traveling wave amplifiers [16]. The Kompfner dip has been successfully used for determining the characteristics of the slow wave structure in TWT interactions.

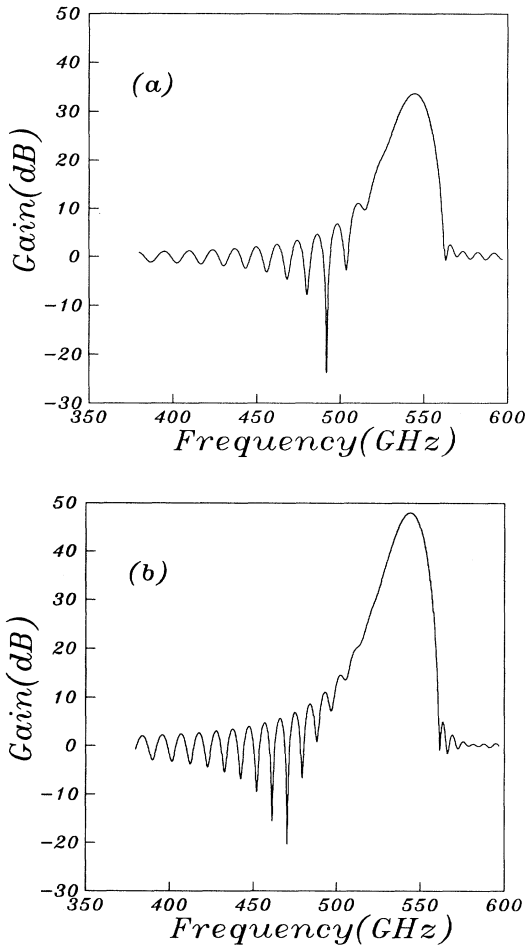

FIG. 6. The gain versus frequency for a TE_{01} mode CARM with an interaction length of (a) 15 cm and (b) 20 cm. Other parameters are the same as in Fig. 1.

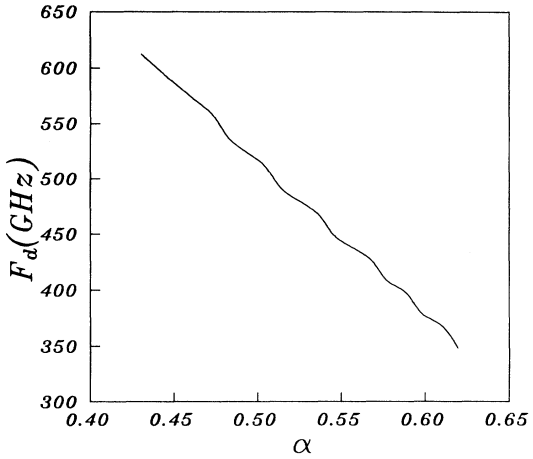

FIG. 7. The frequency for the Kompfner dip as a function of $\alpha(\nu_\perp/\nu_z)$ with $B=110.33$ kG and the interaction length $=17.5$ cm. Other parameters are the same as in Fig. 1.

Therefore, useful information regarding the CARM amplifier can also be provided by determining the conditions for the occurrence of the total absorption of the input signal. For instance, Fig. 7 shows that the Kompfner dip appears at different frequencies for electron beams with different α values. In this figure, since the operating magnetic field is set to be 110.33 kG for each case, the beam mode intersects with the waveguide mode at a higher frequency for lower α and the Kompfner dip subsequently appears for a higher frequency.

V. CONCLUSION

A four-wave linear theory and a self-consistent nonlinear theory are used to investigate the discrepancy between the dispersion relation and the particle simulation code to predict the bandwidth of a CARM amplifier. This discrepancy has previously been attributed to the failure of the linear theory. In contrast, our results show that the dispersion relation is still applicable and valid for a CARM at frequencies not close to the intersection point of the beam mode and the waveguide mode and that the discrepancy is actually due to launching loss effects. The excellent agreement between the linear theory and the self-consistent nonlinear theory proves the adequacy of the dispersion relation and the four-wave model for analyzing the linear behavior of the CARM amplifier.

In addition, the Kompfner dip has also been found to occur in CARM amplifiers. It is due to the beating between the forward constant amplitude wave and the forward growing wave. The condition at which this dip occurs can be used for identifying a CARM's experimental parameters.

ACKNOWLEDGMENTS

This work was supported by the National Science Council (Taiwan, Republic of China) under Contract No. NSC83-0208-N-007-025.

[1] V. L. Bratman, N. S. Ginzburg, G. S. Nusinovich, M. I. Petelin, and P. S. Strelkov, Int. J. Electron. **53**, 555 (1982).
[2] A. T. Lin, Int. J. Electron. **57**, 1097 (1984).
[3] G. Bekefi, A. DiRienzo, C. Leibovitch, and B. G. Danly, Appl. Phys. Lett. **54**, 1302 (1989).
[4] K. D. Pendergast, B. G. Danly, R. J. Temkin, and J. S. Wurtele, IEEE Trans. Plasma Sci. **16**, 122 (1988).
[5] A. DiRienzo, G. Bekefi, C. Chen, and J. S. Wurtele, Phys. Fluids B **3**, 1755 (1990).
[6] J. G. Wang, R. M. Gilgenbach, J. J. Choi, C. A. Outten, and T. A. Spencer, IEEE Trans. Plasma Sci. **17**, 906 (1989).
[7] Q. S. Wang, D. B. McDermott, A. T. Lin, N. C. Luhmann Jr., and K. R. Chu, Int. J. Infrared Millimeter Waves **12**, 297 (1991).
[8] K. R. Chu and J. L. Hirshfield, Phys. Fluids **21**, 461 (1978).
[9] K. R. Chu and A. T. Lin, IEEE Trans. Plasma Sci. **PS-16**, 90 (1988).
[10] J. R. Pierce, *Traveling Wave Tubes* (Van Nostrand, Princeton, N.J., 1950).
[11] C. J. Edgcombe, Int. J. Electron. **51**, 5533 (1981).
[12] J. Y. Choe and S. Ahn, IEEE Trans. Electron Devices **28**, 94 (1981).
[13] C. J. Edgcombe, Int. J. Electron. **48**, 471 (1980).
[14] H. Saito, T. M. Tran, K. E. Kreischer, and R. J. Temkin, Int. J. Electron. **61**, 895 (1986).
[15] H. R. Johnson, Proc. IRE **43**, 874 (1955).
[16] R. Kompfner, J. Brit IRE **10**, 283 (1950).
[17] S. Y. Park, V. L. Granatstein, and R. K. Parker, Int. J. Electron. **37**, 1059 (1980).
[18] C. S. Kou, Ph.D. dissertation, University of California, Los Angeles, 1991.
[19] C. S. Kou, Q. S. Wang, D. B. McDermott, A. T. Lin, K. R. Chu, and N. C. Luhmann, Jr., IEEE Trans Plasma Sci. **20**, 155 (1992).
[20] C. Chen and J. S. Wurtele, Phys. Rev. Lett. **65**, 3389 (1990).
[21] C. Chen and J. S. Wurtele, Phys. Fluids B **3**, 2135 (1991).
[22] A. K. Ganguly and S. Ahn, Int. J. Electron. **53**, 505 (1982).
[23] A. K. Ganguly and S. Ahn, IEEE Trans. Electron Devices **ED-31**, 474 (1984).
[24] A. W. Fliflet, Int. J. Electron. **61**, 1049 (1986).